Supplementary Data

The construction of vanadium-doped polysulfide iron bimetallic active center for enhanced photocatalytic nitrogen fixation

Wei Cai, Kang Li, Jianuan Wen, Zhicheng Zhang, Qin Zhong and Hongxia Qu*

Department of Chemical Engineering and Technology, School of Chemistry and Chemical Engineering, Nanjing University of Science and Technology, Nanjing, Jiangsu 210094, PR China.

* Corresponding author.

E-mail addresses: qhx@mail.njust.edu.cn (H. Qu)

Characterization

The XRD patterns were obtained by an X-ray diffractometer (XRD, Purkinje XD-3, Cu Kα radiation, λ=0.15418 nm). The transmission electron microscopy (TEM) was performed on a Tecnai G2 F30 S-TWIN instrument with an acceleration voltage of 300 kV. Fourier transform infrared (FT-IR) spectroscopy was recorded on a Nicolet-iS10 spectrometer (32 scans). The composition and surface state of the samples were verified by X-ray photoelectron spectroscopy (XPS, PHI QUANTERA II, Al Kα X-ray radiation). The binding energy 284.8 eV was used as the carbon (C–C) correction value. UV–vis diffuse reflectance spectroscopy (DRS) spectra were recorded on a Shimadzu UV-2600 spectrophotometer. N_2-temperature programmed desorption (N_2-TPD) measurements were performed on a ChemiSorb 2040 instrument. Mott–Schottky plots were measured on an electrochemical workstation (CHI 760E, three-electrode system in 0.5 M Na_2SO_4 aqueous solution as an electrolyte). The detection of NO_3^-/NO_2^- conducted using Ion-Chromatography (IC, DIONEX ICS-600, Thermo). The working electrode was fabricated using a drop-casting method. 5 mg of the photocatalysts were dispersed in 1 mL ethanol containing 40 μL Nafion solution (5%) by sonication for 30 min. Then, the dispersive suspension was drop-cast onto a pretreated fluorine-doped tin oxide (FTO) glass substrate, and dried at 60 ℃ in air for 2 h to improve the adhesion. The LC-MS analysis was performed on a high-performance liquid chromatography-mass spectrometry with an Agilent 1290II-6460 Liquid chromatography and waters BEH C18 column (2.1 mm × 100 mm, 1.7 μm). The mobile phase comprised (A) aqueous formic acid (0.1%, v/v) and (B) acetonitrile. Drying gas flow was 12 $L \cdot min^{-1}$. Gas temperature was 350 ℃ and Capillary voltage was 3200V.

In-situ DRIFT experiments were performed on a Nicolet IZ10 spectrometer equipped with a Harrick Scientific DRIFT cell and a Nicolet IZ10 detector. Prior to test, photocatalysts were pretreated at 150 ℃ under N_2 flow (30 mL/min) for 2 h and then cooled to 35 ℃ to get the background spectrum. Next, N_2 (30 mL/min) with bubbled solution (H_2O:CH_3OH=4:1) was introduced into the chamber at 35 ℃ and reacted at

dark for 30 min for adsorption. Then, the light source was turned on to monitor the produced intermediates for another 1 h.

Mott-Schottky plots are analyzed by eq. (1, 2):

$$\frac{1}{C^2} = \frac{2}{e\varepsilon\varepsilon_0 N_D}\left(E - E_{fb} - \frac{KT}{e}\right) \quad (1)$$

$$N_D = \frac{2}{e\varepsilon\varepsilon_0}\left[\frac{d\left(\frac{1}{C^2}\right)}{d(E)}\right]^{-1} \quad (2)$$

Here, C is the differential capacitance of the Helmholtz layer, e represents the charge of single electron (1.602×10^{-19} C), ε is the dielectric of CN, ε_0 is the vacuum permittivity (8.85×10^{-14} F cm^{-1}), E is the applied bias at the electrode, K is the Boltzmann constant (1.38×10^{-23} J K^{-1}), and T is the absolute temperature. Then the flat band potential is obtained by extrapolating the $1/C^2$ value to the x-axis.

Photocatalytic nitrogen fixation

The photocatalytic N_2 fixation was conducted in a 100 mL jacketed reactor with an external circulating water system，which controlled a certain reaction temperature. Briefly, 50 mg of the catalyst was dispersed in 50 mL methanol aqueous solution (20 vol%), and purity nitrogen gas was bubbled into the reaction solution with a flow rate of 30 mL min^{-1}. A 300 W Xe lamp (PLS-SXE300/300UV, working current 15A, output light wavelength 200-2500nm) was turned on as a light source after stirring for 30 min in the dark. At given irradiation time intervals, 2 mL of the reaction solution was taken out and liquid sample was separated by centrifugation at 4200 rpm for 10 min. The

concentration of ammonia was determined by Nessler's reagent method (JB7478-87) with a UV–vis spectrophotometer (T6 New Century, Beijing). The ammonia concentration was calculated by ammonia nitrogen standard curve (Fig. S1). In order to verify that NH_3 is produced from N_2, an experiment was performed by replacing N_2 with Ar. The reaction conditions were the same as for NRR. Before starting the reaction, Ar was introduced in the dark for 1 h to drive off the dissolved nitrogen in the water to avoid the participation of the dissolved nitrogen in the NRR. An Ar atmosphere was then maintained over the solution.

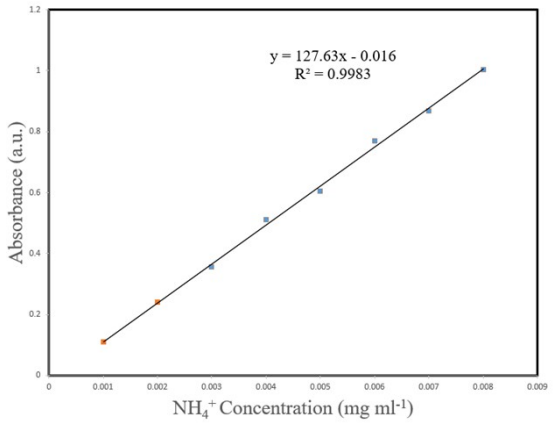

Fig. S1. Ammonia nitrogen standard curve.

Isotopic Labeling Experiment

The isotopic labeling experiment was conducted in a 100 mL photoreactor. 50 mg of wet FeVS@g-C_3N_5 photocatalyst was distributed on the bottom of the photoreactor. Before starting the reaction, Ar was introduced in the dark for 1 h to drive off the air, after which it is completely evacuated by a mechanical pump. Then, $^{15}N_2$ or $^{14}N_2$ gas was injected into the photoreactor, and the FeVS@g-C_3N_5 photocatalyst was exposed to irradiation supplied by a 300 W Xe lamp. After 12 h of visible light irradiation,5 mL

of deionized water was added into the photoreactor to form a mixture solution, which was centrifuged at 5000 rpm. The resulted solution was mixed with 0.2 mL of a phenol solution (1.2 g of phenol in 10 mL a 95% ethanol aqueous solution), 0.2 mL of a 0.5 $g \cdot L^{-1}$ sodium nitroferricyanide dihydrate solution, and 0.7 mL of a NaClO solution (0.1 g of NaOH, 2 g sodium citrate, 1 mL of a 10 wt % NaClO solution in 10 mL of deionized water) and stirred for 1 h. The indophenol in the mixture solution was then analyzed by HPLC/MS (Agilent 1290II-6460) system with a waters BEH C 18 column [1].

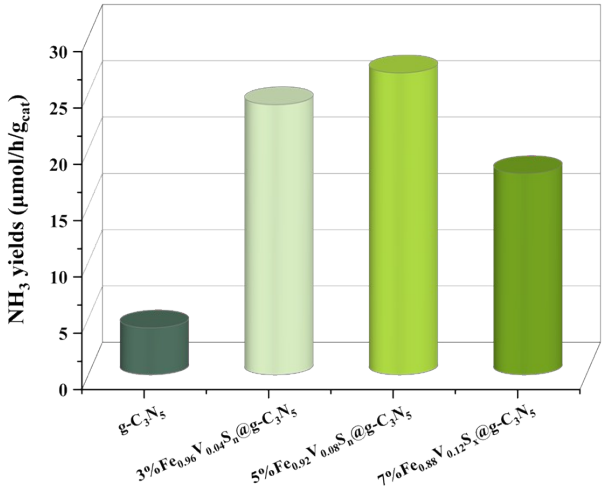

Fig. S2. NH_3 yields of samples with different polysulfide loadings.

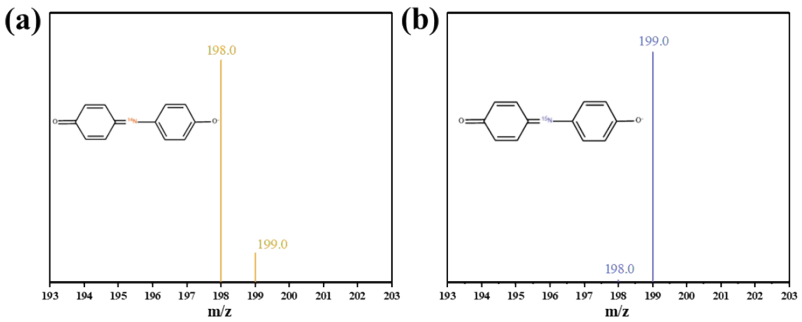

Fig. S3. Mass spectra of the product (indophenol) produced by reaction of phenol with NH_3 generated from photocatalytic (a) $^{14}N_2$ or (b) $^{15}N_2$ reduction. The inset is the chemical structure of the indophenol product, with m/z = 198.0 (indophenol containing ^{14}N) and m/z = 199.0 (indophenol containing ^{15}N).

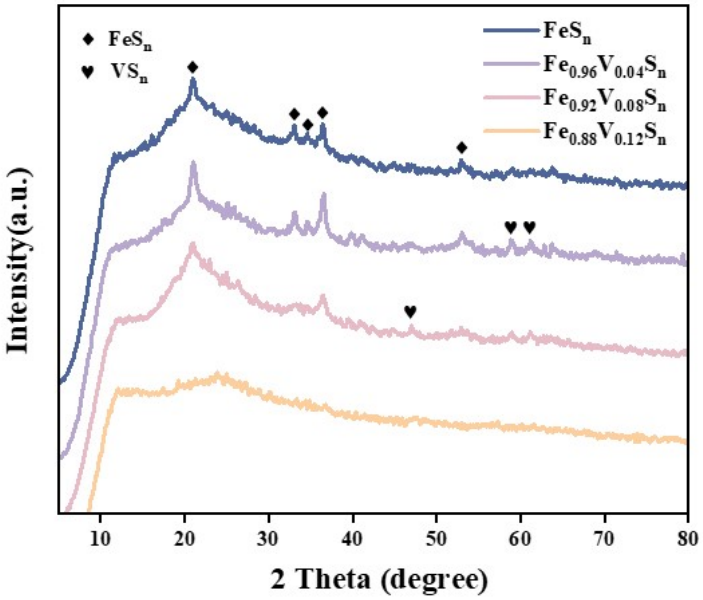

Fig. S4. XRD patterns of FeVS.

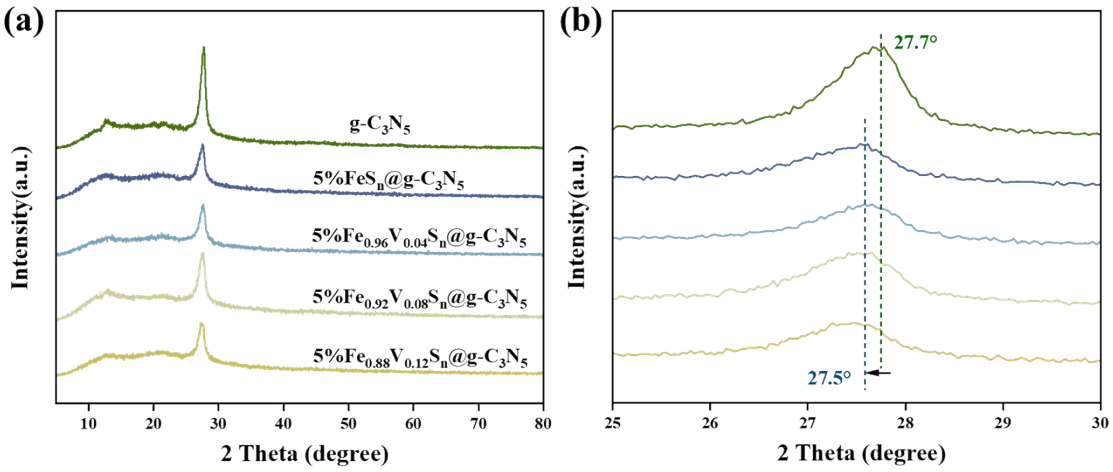

Fig. S5. XRD patterns of (a) g-C_3N_5 and samples with different polysulfide loadings and (b) partial enlargement diagram of XRD patterns.

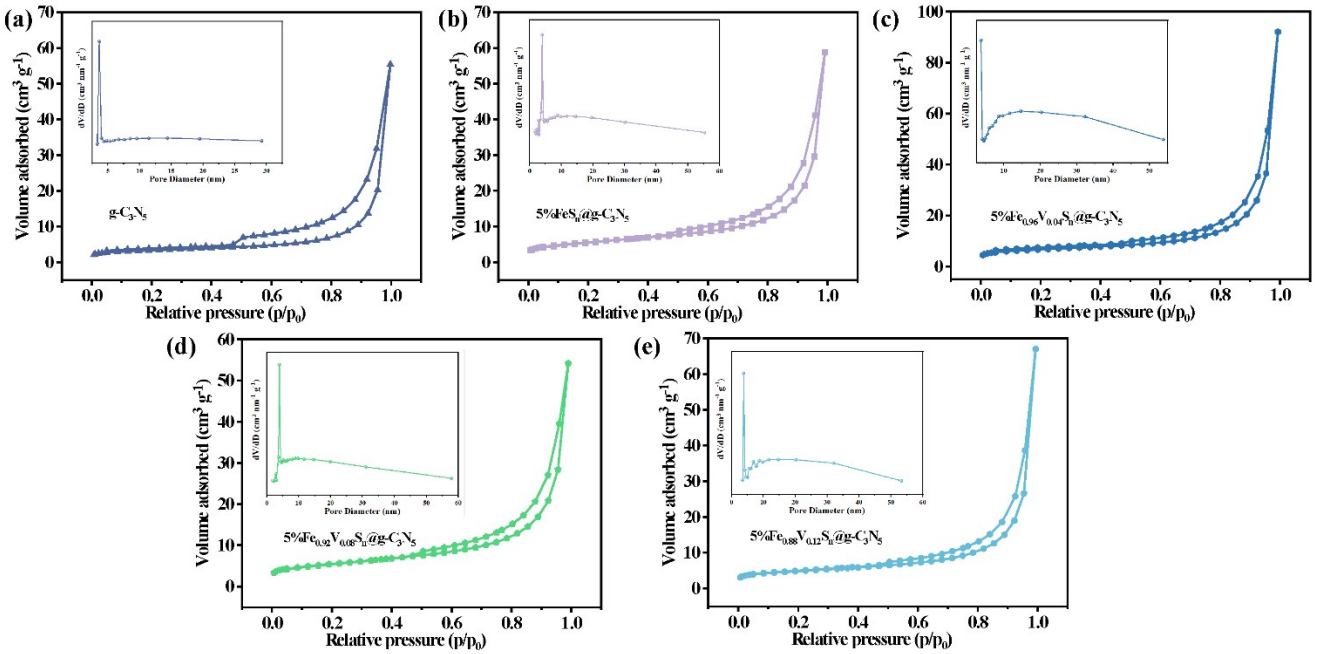

Fig. S6. N_2 adsorption-desorption isotherms of all samples (Insert was the corresponding BJH mesopore size distributions).

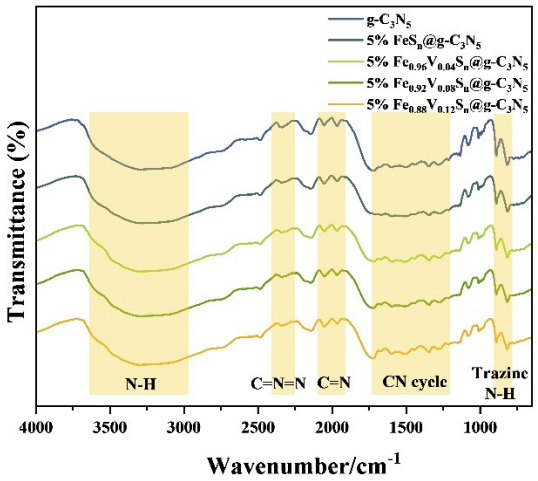

Fig. S7. FT-IR of all samples.

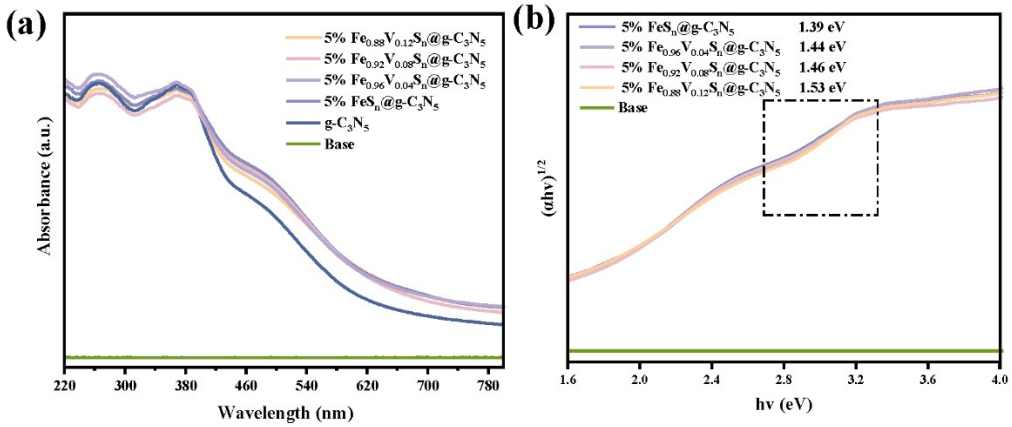

Fig. S8. (a) UV–vis DRS spectra and (b) tauc plots for samples.

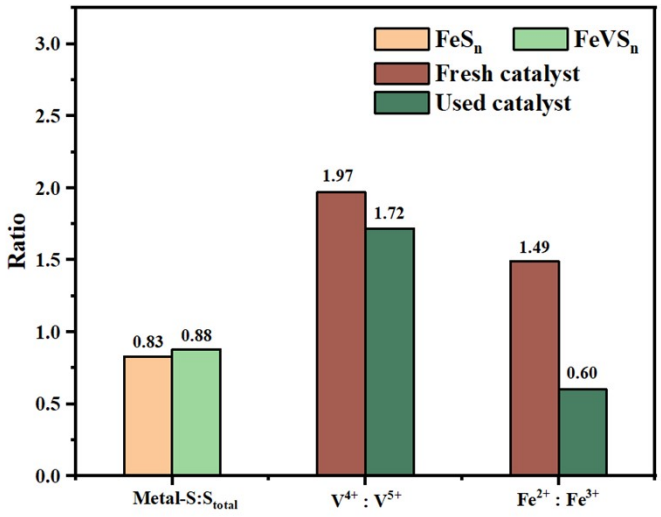

Fig. S9. XPS data analysis.

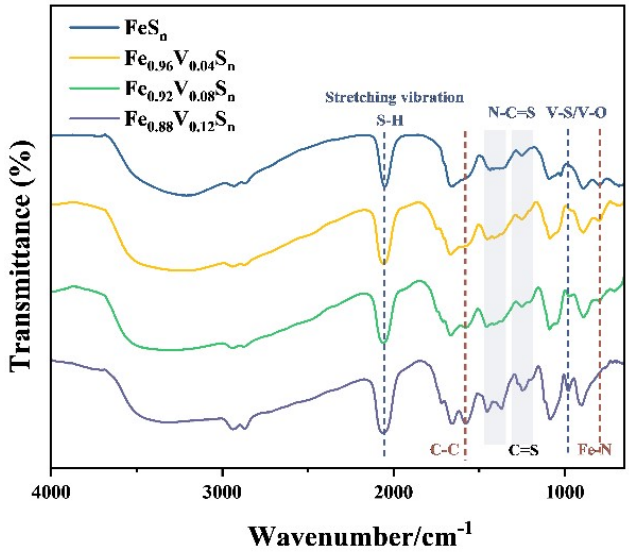

Fig. S10. FT-IR of FeVS.

Tab. S1. Performance comparison of the reported photocatalysts for NRR.

	Photocatalyst	Activity	Light source	Reference
This work	FeVS@g-C_3N_5	1916.5 μmol·h^{-1}·$g_{cat.}^{-1}$	300W Xe lamp	
Iron modified catalysts	FeN-CDs/TiO_2@CN	9.365 mg·h^{-1}·g_{cat}^{-1}	300W Xe lamp	[2]
	GF (Fe_2O_3 loaded g-C_3N_4)	47.9 mg/L/h	300W Xe lamp	[3]
	Al-PMOF(Fe)	127 μg·h^{-1}·g_{cat}^{-1}	AM 1.5G	[4]
	Fe-Bi_2MoO_6	106.5 μmol·h^{-1}·g^{-1}	300W Xe lamp	[5]
	MIL-53(FeII/FeIII)	306 μmol·h^{-1}·g^{-1}	300W Xe lamp	[6]
	Fe doped $SrMoO_4$	93.1μmol·h^{-1}·g^{-1}	300W Xe lamp	[7]
Carbon Nitride	Ti_3C_2/N-defect g-C_3N_4 nanosheets	5.792 mg·h^{-1}·g_{cat}^{-1}	300W Xe lamp	[8]
	C_3N_4/r-Ti_3C_2 QD	328.9 μmol·h^{-1}·g^{-1}	300W Xe lamp	[9]
	B-doping in g-C_3N_4(BCN)	313.9 μmol·h^{-1}·g^{-1}	250W Xe lamp	[10]
	Bi-defective g-C_3N_4 (K and -Ctriple bond≡N) nanorod	23.5 mmol/(h·g_{cat})	300W Xe lamp	[11]
	B-C_3N_5	421.18 μmol·h^{-1}·g^{-1}	300W Xe lamp	[12]
	NV-g-C_3N_5/BiOBr	29.4 μg·h^{-1}·mg^{-1}	300W Xe lamp	[13]
Sulfides	g-C_3N_4/ZnMoCdS	3.5 mg·L^{-1}·h^{-1}·g_{cat}^{-1}	500W Xe lamp	[14]
	g-C_3N_4/ZnSnCdS	7.543mg·L^{-1}·h^{-1}·g_{cat}^{-1}	250W Xe lamp	[15]
	MoS_2	325 μmol·h^{-1}·g^{-1}	500W Xe lamp	[16]
	WS_2@TiO_2	1.39 mmol·h^{-1}·g^{-1}	AM 1.5G	[17]
	In_2S_3 nanotubes	52.49 μmol·h^{-1}·g^{-1}	300W Xe lamp	[18]
	$Zn_3In_2S_6$ nanosheets	355.2 mg·L^{-1}·h^{-1}·g_{cat}^{-1}	300W Xe lamp	[19]
	SV-1T-MoS_2-/CdS	8220.83 μmol·L^{-1}·h^{-1}·g^{-1}	AM 1.5G	[20]
	Pt/N-MoS_2	133.8 μmol·h^{-1}·g_{cat}^{-1}	300 W Xe lamp	[21]
Nitrogenase Biomimetic	TiO_2/Mo_2C@C	432 μg·g_{cat}^{-1}·h^{-1}	300W Xe lamp	[22]
	UiO-66 (Zr-Hf)	351.8 μmol·h^{-1}·g^{-1}	300W Xe lamp	[23]
	MIL-88A(Fe/Mo_x)/Fe mesh	2.30 × 10^{-2} μmol/cm^2/h	350W Xe lamp	[24]
	Fe/Mo–BMWO	218.93 μmol·h^{-1}·g^{-1}	300W Xe lamp	[25]
	Fe–$MoTe_2$	129.08 μmol·h^{-1}·g^{-1}	300W Xe lamp	[26]

Reference

[1] Yuan, Y.J.; Lu, N.; Bao, L.; Tang, R.; Zhang, F.G.; Guan, J.; Wang, H.D.; Liu, Q.Y.; Cheng, Q.; Yu, Z.T.; Zou, Z. SiP Nanosheets: A Metal-Free Two-Dimensional Photocatalyst for Visible-Light Photocatalytic H(2) Production and Nitrogen Fixation, *ACS Nano*, **2022**, *16*, 12174-12184.

[2] Li, K.; Sun, C.; Chen, Z.; Qu, H.; Xie, H.; Zhong, Q. Fe-carbon dots enhance the photocatalytic nitrogen fixation activity of TiO2@CN heterojunction, *Chem. Eng. J.*, **2022**, *429*, 132440.

[3] Liu, S.; Wang, S.; Jiang, Y.; Zhao, Z.; Jiang, G.; Sun, Z. Synthesis of Fe2O3 loaded porous g-C3N4 photocatalyst for photocatalytic reduction of dinitrogen to ammonia, *Chem. Eng. J.*, **2019**, *373*, 572-579.

[4] Shang, S.; Xiong, W.; Yang, C.; Johannessen, B.; Liu, R.; Hsu, H.-Y.; Gu, Q.; Leung, M.K.H.; Shang, J. Atomically Dispersed Iron Metal Site in a Porphyrin-Based Metal–Organic Framework for Photocatalytic Nitrogen Fixation, *ACS Nano*, **2021**, *15*, 9670-9678.

[5] Meng, Q.; Lv, C.; Sun, J.; Hong, W.; Xing, W.; Qiang, L.; Chen, G.; Jin, X. High-efficiency Fe-Mediated Bi2MoO6 nitrogen-fixing photocatalyst: Reduced surface work function and ameliorated surface reaction, *Appl. Catal., B*, **2019**, *256*, 117781.

[6] Zhao, Z.; Yang, D.; Ren, H.; An, K.; Chen, Y.; Zhou, Z.; Wang, W.; Jiang, Z. Nitrogenase-inspired mixed-valence MIL-53(FeII/FeIII) for photocatalytic nitrogen fixation, *Chem. Eng. J.*, **2020**, *400*, 125929.

[7] Luo, J.; Bai, X.; Li, Q.; Yu, X.; Li, C.; Wang, Z.; Wu, W.; Liang, Y.; Zhao, Z.; Liu, H. Band structure engineering of bioinspired Fe doped SrMoO4 for enhanced photocatalytic nitrogen reduction performance, *Nano Energy*, **2019**, *66*, 104187.

[8] Sun, C.; Chen, Z.; Cui, J.; Li, K.; Qu, H.; Xie, H.; Zhong, Q. Site-exposed Ti3C2 MXene anchored in N-defect g-C3N4 heterostructure nanosheets for efficient photocatalytic N2 fixation, *Catalysis Science & Technology*, **2021**, *11*, 1027-1038.

[9] Chang, B.; Guo, Y.; Liu, H.; Li, L.; Yang, B. Engineering a surface defect-rich Ti3C2 quantum dots/mesoporous C3N4 hollow nanosphere Schottky junction for efficient N2 photofixation, *Journal of Materials Chemistry A*, **2022**, *10*, 3134-3145.

[10] Wang, W.; Zhou, H.; Liu, Y.; Zhang, S.; Zhang, Y.; Wang, G.; Zhang, H.; Zhao, H. Formation of B□N□C Coordination to Stabilize the Exposed Active Nitrogen Atoms in g-C3N4 for Dramatically Enhanced Photocatalytic Ammonia Synthesis Performance, *Small*, **2020**, *16*, 1906880.

[11] Liu, G.; Tang, Z.; Gu, X.; Li, N.; Lv, H.; Huang, Y.; Zeng, Y.; Yuan, M.; Meng, Q.; Zhou, Y.; Wang, C. Boosting photocatalytic nitrogen reduction to ammonia by dual defective -CN and K-doping sites on graphitic carbon nitride nanorod arrays, *Appl. Catal., B*, **2022**, *317*, 121752.

[12] Li, K.; Cai, W.; Zhang, Z.; Xie, H.; Zhong, Q.; Qu, H. Boron doped C3N5 for photocatalytic nitrogen fixation to ammonia: The key role of boron in nitrogen activation and mechanism, *Chem. Eng. J.*, **2022**, *435*, 135017.

[13] Li, M.; Lu, Q.; Liu, M.; Yin, P.; Wu, C.; Li, H.; Zhang, Y.; Yao, S. Photoinduced Charge Separation via the Double-Electron Transfer Mechanism in Nitrogen Vacancies g-C3N5/BiOBr for the Photoelectrochemical Nitrogen Reduction, *ACS Applied Materials & Interfaces*, **2020**, *12*, 38266-38274.

[14] Zhang, Q.; Hu, S.; Fan, Z.; Liu, D.; Zhao, Y.; Ma, H.; Li, F. Preparation of g-C3N4/ZnMoCdS hybrid heterojunction catalyst with outstanding nitrogen photofixation performance under visible light via hydrothermal post-treatment, *Dalton Transactions*, **2016**, *45*, 3497-3505.

[15] Hu, S.; Li, Y.; Li, F.; Fan, Z.; Ma, H.; Li, W.; Kang, X. Construction of g-C3N4/Zn0.11Sn0.12Cd0.88S1.12 Hybrid Heterojunction Catalyst with Outstanding Nitrogen Photofixation Performance Induced by

Sulfur Vacancies, *ACS Sustainable Chemistry & Engineering*, **2016**, *4*, 2269-2278.
[16] Sun, S.; Li, X.; Wang, W.; Zhang, L.; Sun, X. Photocatalytic robust solar energy reduction of dinitrogen to ammonia on ultrathin MoS2, *Appl. Catal., B*, **2017**, *200*, 323-329.
[17] Shi, L.; Li, Z.; Ju, L.; Carrasco-Pena, A.; Orlovskaya, N.; Zhou, H.; Yang, Y. Promoting nitrogen photofixation over a periodic WS2@TiO2 nanoporous film, *Journal of Materials Chemistry A*, **2020**, *8*, 1059-1065.
[18] He, Z.; Wang, Y.; Dong, X.; Zheng, N.; Ma, H.; Zhang, X. Indium sulfide nanotubes with sulfur vacancies as an efficient photocatalyst for nitrogen fixation, *RSC Advances*, **2019**, *9*, 21646-21652.
[19] Han, H.; Yang, Y.; Liu, J.; Zheng, X.; Wang, X.; Meng, S.; Zhang, S.; Fu, X.; Chen, S. Effect of Zn Vacancies in Zn3In2S6 Nanosheets on Boosting Photocatalytic N2 Fixation, *ACS Applied Energy Materials*, **2020**, *3*, 11275-11284.
[20] Sun, B.; Liang, Z.; Qian, Y.; Xu, X.; Han, Y.; Tian, J. Sulfur Vacancy-Rich O-Doped 1T-MoS2 Nanosheets for Exceptional Photocatalytic Nitrogen Fixation over CdS, *ACS Applied Materials & Interfaces*, **2020**, *12*, 7257-7269.
[21] Maimaitizi, H.; Abulizi, A.; Zhang, T.; Okitsu, K.; Zhu, J.-j. Facile photo-ultrasonic assisted synthesis of flower-like Pt/N-MoS2 microsphere as an efficient sonophotocatalyst for nitrogen fixation, *Ultrason. Sonochem.*, **2020**, *63*, 104956.
[22] Chen, L.C.; Shou, J.X.; Chen, Y.T.; Han, W.H.; Tu, X.W.; Zhang, L.P.; Sun, Q.; Cao, J.; Chang, Y.R.; Zheng, H. Efficient sunlight promoted nitrogen fixation from air under room temperature and ambient pressure via Ti/Mo composites, *Chem. Eng. J.*, **2023**, *451*, 138592.
[23] An, K.; Ren, H.J.; Yang, D.; Zhao, Z.F.; Gao, Y.C.; Chen, Y.; Tan, J.D.; Wang, W.J.; Jiang, Z.Y. Nitrogenase-inspired bimetallic metal organic frameworks for visible-light-driven nitrogen fixation, *Applied Catalysis B-Environmental*, **2021**, *292*, 120167.
[24] Wang, W.; Qu, J.; Li, C.; Guo, L.; Fang, X.; Chen, G.; Duan, J. “MoFe cofactor” inspired iron mesh-based MIL-88A(Fe/Mo) for bionic photocatalytic nitrogen fixation, *Molecular Catalysis*, **2022**, *532*, 112730.
[25] Li, H.; Deng, H.; Gu, S.; Li, C.; Tao, B.; Chen, S.; He, X.; Wang, G.; Zhang, W.; Chang, H. Engineering of bionic Fe/Mo bimetallene for boosting the photocatalytic nitrogen reduction performance, *J. Colloid Interface Sci.*, **2022**, *607*, 1625-1632.
[26] Li, H.; Gu, S.; Sun, Z.; Guo, F.; Xie, Y.; Tao, B.; He, X.; Zhang, W.; Chang, H. The in-built bionic “MoFe cofactor” in Fe-doped two-dimensional MoTe2 nanosheets for boosting the photocatalytic nitrogen reduction performance, *Journal of Materials Chemistry A*, **2020**, *8*, 13038-13048.

Tab. S2. Specific surface area and pore structure of all samples.

	BET Surface Area（m^2/g）	**Pore volume（cm^3/g）**	**Pore size（nm）**
g-C_3N_5	11.2035	0.026281	11.0568
5%FeS_n@g-C_3N_5	19.3733	0.037705	17.6748
5%$Fe_{0.96}V_{0.04}S_n$@g-C_3N_5	22.3047	0.049250	25.0848
5% $Fe_{0.92}V_{0.08}S_n$ @g-C_3N_5	19.0077	0.038909	17.4327
5% $Fe_{0.88}V_{0.12}S_n$ @g-C_3N_5	16.2998	0.035489	23.5731